NJC

RSC Publishing

PAPER

View Article Online
View Journal | View Issue

Cite this: *New J. Chem.*, 2013, **37**, 1782

Preparation and photodynamic therapy application of $NaYF_4$:Yb, Tm–$NaYF_4$:Yb, Er multifunctional upconverting nanoparticles†

Xiaolan Chen,* Zengxia Zhao, Mengying Jiang, Daiping Que, Saige Shi and Nanfeng Zheng*

Received (in Montpellier, France) 15th January 2013,
Accepted 4th April 2013

DOI: 10.1039/c3nj00065f

www.rsc.org/njc

The preparation, characterization and application of $NaYF_4$:Yb^{3+}, Tm^{3+}–$NaYF_4$:Yb^{3+}, Er^{3+} core–shell upconversion nanocrystals (UCNPs) with multiple emission peaks (*e.g.* 539, 654 and 802 nm) have been demonstrated in this work. The monodisperse nanocrystals were prepared *via* a modified thermal decomposition synthesis. The resulting UCNPs were ~31 nm in diameter with the lanthanide ions Tm^{3+} and Er^{3+} doped in the core and the shell, respectively. Under the laser diode excitation at 980 nm, these core–shell nanocrystals give strong upconversion emissions from the visible to near-infrared (NIR) region. By coating a PEG–phospholipid (PP) layer on the surface of the nanocrystals, the as-prepared UCNPs were favorably endowed with good water solubility for the potential biological applications. Here, a photosensitizer drug of Chlorin e6 (Ce6), which has maximum absorption that overlaps with the red emission of UCNPs, was loaded on these PP-coated UCNPs (UCNP@PP) by physical adsorption. The activity of the Ce6-loaded UCNP@PP (UCNP@PP–Ce6) in photodynamic therapy of cancer cells *in vitro* has been fully investigated in this work. Our results indicated that these multifunctional UCNP@PP–Ce6 nanoparticles have efficient NIR-to-NIR upconversion luminescence and photodynamic therapy capabilities, which could be potentially employed as a theranostic platform for cancer treatment.

1. Introduction

In recent years, multifunctional nanomaterials have attracted great interest in biomedical studies due to their capabilities to integrate various functionalities, such as targeting, imaging, drug delivery and therapy, into one single entity.[1–13] Among them, lanthanide (Ln^{3+})-doped upconversion nanoparticles (UCNPs) are promising candidates as a highly efficient diagnosis and therapy platform owing to their attractive features: (1) their absorbance at near-infrared (NIR) wavelengths allows for tissue penetration to a depth of centimeters and reduces autofluorescence from biological tissue;[14–18] (2) their emitting wavelength can be fine-tuned by changing the host matrix and lanthanide dopants;[19,20] (3) UCNPs possess high quantum yields, narrow emission peaks, large Stokes shifts, low toxicity, good chemical stability and photostability.[23] Due to these promising advantages of the UCNPs, intensive investigations have been carried out to explore the preparation of varieties of UCNPs and their applications in detection, bioimaging, therapy and optical limiting *etc.*[10–31] Especially, as the "optical transmission window" of the biological tissues is in the NIR range (700–1000 nm), where blood and tissue are maximally transparent and the NIR light can penetrate several centimeters in depth, the UCNPs with NIR excitation and NIR emission are greatly favoured for both *in vitro* and *in vivo* imaging. As a result, different Tm^{3+}-doped UCNP platforms with NIR-to-NIR upconversion luminescence have been developed previously for high contrast and highly penetrating *in vivo* fluorescence imaging.[27,28,32]

The prominent optical properties of UCNPs also break a new path for current PDT. It has been reported that the NIR light-triggered photodynamic therapy (PDT) could effectively reduce the photosensitivity to ambient light and improve the safety of PDT.[30] The NIR excitation of UCNPs permits deeper tissue penetration than visible light, which is suitable for the PDT of deep tissue cancer.[33] In addition, the visible upconversion luminescence from the excited UCNPs can overlap the maximum absorption of many available photosensitizers (PSs). Therefore, this light can be utilized to activate surrounding PSs to produce reactive

State Key Laboratory of Physical Chemistry of Solid Surfaces and Department of Chemistry, College of Chemistry and Chemical Engineering, Xiamen University, Xiamen 361005, PR China. E-mail: chenxl@xmu.edu.cn, nfzheng@xmu.edu.cn

† Electronic supplementary information (ESI) available: SEM images of the $NaYF_4$:Yb^{3+}, Tm^{3+} core nanocrystals and the corresponding size statistics obtained from the SEM results, EDX results of the $NaYF_4$:Yb^{3+}, Tm^{3+} core and the $NaYF_4$:Yb^{3+}, Tm^{3+}–$NaYF_4$:Yb^{3+}, Er^{3+} core–shell nanocrystals (UCNPs), FTIR spectra of DSPE-PEG2000 (PP), some control experiments on optical imaging of 7703 liver cancer cells stained with trypan blue. See DOI: 10.1039/c3nj00065f

oxygen species to kill cancer cells.[30,33–43] Zhang and coworkers first reported the representative application of $NaYF_4$ UCNPs in PDT.[34] Later, several groups have modified UCNPs by coating a silica layer or an amphiphilic polymer for synergistic optical, MRI imaging and PDT applications.[30,33,35–43] However, the previous investigation of upconverting nanoparticles in both imaging and PDT is mainly based on the Yb^{3+}/Er^{3+} co-doped $NaYF_4$ or $NaGdF_4$ UCNPs.[30,33–43] As Yb^{3+}/Er^{3+} co-doped $NaYF_4$ usually gives a bright green emission (around 550 nm) along with a weak dark red emission (around 660 nm), its tissue imaging applications are greatly restricted owing to the shallow penetration depth of green light and the low intensity of red emission whose signal is usually too weak to be detected.[24,29] Therefore, it is highly desired to synthesize Er^{3+} and Tm^{3+}co-doped UCNPs with multiple emissions that can be applied for both NIR imaging and PDT.

Herein we report the use of a thermal decomposition method to synthesize $NaYF_4$:Yb^{3+}, Tm^{3+}–$NaYF_4$:Yb^{3+}, Er^{3+} core–shell nanocrystals with Tm^{3+} and Er^{3+} doped in the core and the shell, respectively. The morphologies of the core–shell nanocrystals were characterized using SEM and TEM. A PEG–phospholipid layer was then coated on the surface of UCNPs (UCNPs@PP) to render them water-soluble. The UCNPs displayed strong NIR-to-visible (500–700 nm) and NIR-to-NIR (750–850 nm) upconversion fluorescence under the excitation of the 980 nm laser. The visible emission can be used to activate photosensitizers for PDT and the NIR emission can be utilized for image tracking. The application of the UCNPs@PP nanoparticles as carriers for photosensitizer Ce6 in the photodynamic destruction of cancer cells *in vitro* was investigated in detail.

2. Experimental section

2.1 Chemicals

Re_2O_3 (Re = Y, Yb, Er and Tm, 99.99%), trifluoroacetic acid (CF_3COOH, 99%), sodium trifluoroacetate (CF_3COONa, 98%), 3-[4,5-dimethylthiazol-2-yl]-2,5-diphenyltetrazolium bromide (MTT) and 1,3-diphenylisobenzofuran (DPBF) were purchased from Sigma-Aldrich. Oleic acid (technical grade, 90%) and 1-octadecene (technical grade, 90%) were purchased from Alfa Aesar. 1,2-Distearoyl-*sn-glycero*-3-phosphoethanolamine-*N*-[methoxy(polyethylene glycol)-2000] (mPEG-2000 PE, PP) was obtained from Avanti Polar Lipids, Inc. Chlorin e6 (Ce6, >95%) was purchased from Frontier Scientific, Inc. All the $Re(CF_3COO)_3$ precursors were prepared by dissolving the corresponding rare-earth oxides in CF_3COOH–water (1 : 1) solutions and heating at the refluxing temperature until the solution became clear. All other chemicals were of analytical-reagent grade and used without further purification. The water used in all experiments was ultrapure.

2.2 Synthesis of $NaYF_4$:Yb^{3+}, Tm^{3+}–$NaYF_4$:Yb^{3+}, Er^{3+} core–shell nanocrystals (UCNPs)

The synthesis was carried out under standard oxygen-free conditions. In a typical procedure, the $NaYF_4$:Yb^{3+}, Tm^{3+} core solution was prepared by mixing 1.25 mmol of $Re(CF_3COO)_3$ (Y : Yb : Tm = 69.5% : 30% : 0.5%) and 1.25 mmol of CF_3COONa in 2.5 ml of 1-octadecene and 5 ml of oleic acid (denoted A). The $NaYF_4$:Yb^{3+}, Er^{3+} shell solution was prepared by mixing 1.25 mmol of $Re(CF_3COO)_3$ (Y : Yb : Er = 78% : 20% : 2%) and 1.25 mmol of CF_3COONa in another reaction vessel with 2.5 ml of 1-octadecene and 5 ml of oleic acid (denoted B). 15 ml of 1-octadecene and 10 ml of oleic acid were then prepared in a 100 ml three-neck round bottom flask (denoted C). A and C were heated to 125 °C under an argon blanket with stirring for 30 min to remove residual water and oxygen. The solution of C was then heated to 305 °C under argon and maintained at this temperature. The solution of A at 125 °C was then transferred dropwise into C using a syringe pump at a flow rate of 1.0 ml min^{-1} (KDS100, USA). After completing the addition, the reaction mixture was heated to 320 °C and kept at this temperature for 30 min to form the $NaYF_4$:Yb^{3+}, Tm^{3+} core. Then the shell precursors (solution B) at 125 °C were injected (at a rate of 1.0 ml min^{-1}) into the above reaction vessel C which contains the core nanoparticles. While delivering B, C was maintained at 305 °C. After completing the addition, the reaction mixture was heated to 320 °C and kept at this temperature for 30 min under argon. Subsequently, solution C was allowed to cool to room temperature. Nanocrystals were precipitated out by adding ethanol and were isolated *via* centrifugation (12 000 rpm, 6 min). The products were washed with a 1 : 8 cyclohexane–ethanol (V/V) mixture three times to remove any impurities. The as-prepared nanocrystals could be easily re-dispersed in cyclohexane or chloroform.

The synthetic process of the core-only nanocrystals ($NaYF_4$:Yb^{3+}, Tm^{3+}) was similar to that of the core–shell nanocrystals. Lanthanide trifluoroacetate precursors and sodium trifluoroacetic acid (in stoichiometric quantities) were dissolved in 2.5 ml of 1-octadecene and 5.0 ml of oleic acid (solution A). Following degassing, the solution was injected into the reaction vessel which contains 25 ml of degassed oleic acid and 1-octadecene (solution B) at 305 °C under Ar and heated for 30 min at 320 °C. All subsequent steps were identical.

2.3 Modification of UCNPs with PEG–phospholipids (UCNP@PP)

Briefly, 1 ml of UCNPs dispersed in chloroform (10 mg ml^{-1}) was mixed with 2 ml of mPEG-2000 PE (PP) in chloroform (10 mg ml^{-1}) and stirred for 2 h. Then a lab rotary evaporator with a water bath at 60 °C was used to evaporate the solvent and the residue was readily dispersed in water. The resulting dispersion was filtered through a 0.22 μm cellulose acetate syringe filter to remove large aggregates and kept at 4 °C for further use.

2.4 Loading Chlorin e6 on UCNP@PP (UCNP@PP–Ce6)

The loading of Chlorin e6 onto the UCNP@PP was carried out by mixing Ce6 (0.8 μmol) with UCNP@PP (0.5 mg ml^{-1}) in phosphate buffer solution (PBS, pH = 7.4) for 24 h at room temperature. Free Ce6 was removed by centrifugation at 14 000 rpm for 10 min and washed 3 times with PBS buffer. The formed composite was re-dispersed in PBS and stored at 4 °C. A detailed scheme for the preparation of UCNP@PP–Ce6 is illustrated in Scheme 1.

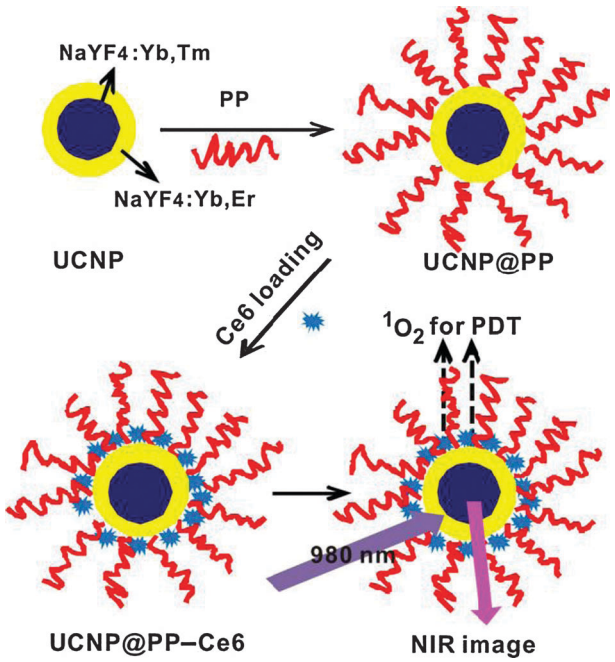

Scheme 1 Synthesis of UCNP@PP–Ce6 nanoparticles.

The concentrations of Ce6 loaded onto UCNP@PP were determined by the absorbance at 404 nm with the UCNP@PP as a blank reference.

2.5 Determination of singlet oxygen

Singlet oxygen production was determined using 1,3-diphenylisobenzofuran (DPBF) as a chemical $^1O_2$ probe, which reacted irreversibly with $^1O_2$ to cause a decrease in the DPBF absorption intensity at about 400 nm.[44] In a typical experiment, 30 μl of DPBF (1.5 mg ml^{-1} in acetonitrile) was added into a solution of UCNP@PP–Ce6 in acetonitrile (2 ml). The solutions were then irradiated with a 980 nm laser for 30 min, and the absorption intensity of DPBF at 420 nm was recorded at given time intervals. UCNP@PP in acetonitrile mixed with DPBF was used as the control experiment.

2.6 Cellular experiments

2.6.1 Cell culture. The human hepatoma cells (QGY-7703), human hepatocytes (QSG-7701) and HeLa cells were obtained from the cell store room of Chinese Academy of Science. Cells were grown in normal RPMI-1640 culture medium with 10% calf serum, 100 U ml^{-1} penicillin and 100 μg ml^{-1} streptomycin at 37 °C, in an incubator with a 5% CO_2 atmosphere.

2.6.2 Cytotoxicity of UCNP@PP–Ce6. The *in vitro* cytotoxicities of UCNP@PP–Ce6 to normal cells and cancer cells were evaluated using a standard methyl thiazolyl tetrazolium (MTT) assay. Briefly, the QGY-7703 and QSG-7701 cells were seeded into 96-well cell-culture plates (Nunc™) at ~10^4 per well and incubated for 24 h at 37 °C under 5% CO_2. Various concentrations of UCNP@PP–Ce6 (0, 50, 100, 200, 500 μg ml^{-1}, diluted in the RPMI 1640 media) were then added to the wells. The cells were further incubated for 12 h. Subsequently, the MTT solution (25 μl, 5 mg ml^{-1}) was added to each well and incubated for an additional 4 h at 37 °C. Then the formazan product was dissolved in 150 μl dimethylsulfoxide (DMSO) solution. After 10 min, the absorbance at 490 nm for each well was recorded on a Tecan Infinite M 200 monochromator-based multifunction microplate reader. The corresponding nanoparticles with cells but not treated by MTT were used as controls.

2.6.3 Uptake of UCNP@PP–Ce6 by cells. To test the uptake of UCNP@PP–Ce6 nanoparticles by cells, HeLa cells were chosen and cultured in 35 mm culture dishes for 24 h. Then the culture medium was replaced by medium containing 200 μg ml^{-1} UCNP@PP–Ce6 nanoparticles. After 4 h incubation, the cells were washed three times with the PBS buffer. Confocal fluorescence imaging was performed using an Olympus Fluoview 1000 laser-scanning microscope and a 100× oil-immersion objective lens. A 405 nm laser was used to excite the nanoparticles, and the fluorescence of Ce6 was collected in a range of 600–750 nm.

2.6.4 *In vitro* photodynamic therapy. For the photodynamic cancer cell killing, QGY-7703 was seeded onto a 24-well plate with a density of 10^5 cells per well and incubated for 24 h. Then the medium was replaced by cell medium (0.5 ml per well) containing 100 μg ml^{-1} of UCNP@PP–Ce6, UCNP@PP, or free Ce6. After incubation for 12 h, the cells were washed with PBS three times to remove the unbound nanoparticles. Then 0.5 ml PBS was added and the cells were exposed to a 980 nm laser with a power density of 1.5 W cm^{-2} for 5 min, respectively. After staining with trypan blue, the optical imaging was performed using the fluorescence microscopy.

2.7 Characterization

The size and morphologies of nanoparticles were determined at 300 kV using a TECNAI F-30 high-resolution transmission electron microscope. Energy-dispersive X-ray analysis (EDXA) of the samples was also performed during high-resolution TEM measurements. X-ray diffraction (XRD) measurements were recorded on a PANalytical X'pert PRO diffractometer using Cu Kα radiation, operating at 40 kV and 30 mA. UV-Visible (UV-Vis) absorption spectra were obtained using a UV 2550 spectrophotometer. The upconversion luminescence emission spectra were recorded on a USB 2000 VIS-NIR spectrometer (Ocean Optics), using an external 0–5 W adjustable 980 nm semiconductor laser (BWT Beijing Ltd) as the excitation source. Dynamic light scattering (DLS) and zeta potential experiments were carried out on a Nano-ZS (Malvern Instruments).

3. Results and discussion

3.1 Synthesis and characterization of $NaYF_4$:Yb^{3+}, Tm^{3+}–$NaYF_4$:Yb^{3+}, Er^{3+} core–shell nanocrystals

The $NaYF_4$:Yb^{3+}, Tm^{3+}–$NaYF_4$:Yb^{3+}, Er^{3+} core–shell nanocrystals (UCNPs) were prepared using a modified thermal decomposition process.[18,45,46] Briefly, the core precursors (the lanthanide (Y, Yb and Tm) trifluoroacetate and sodium trifluoroacetate) dissolved in a small amount of 1-octadecene and oleic acid were firstly injected using a syringe pump into a hot solution of oleic acid and 1-octadecene. After the $NaYF_4$:Yb^{3+}, Tm^{3+} core nanocrystals

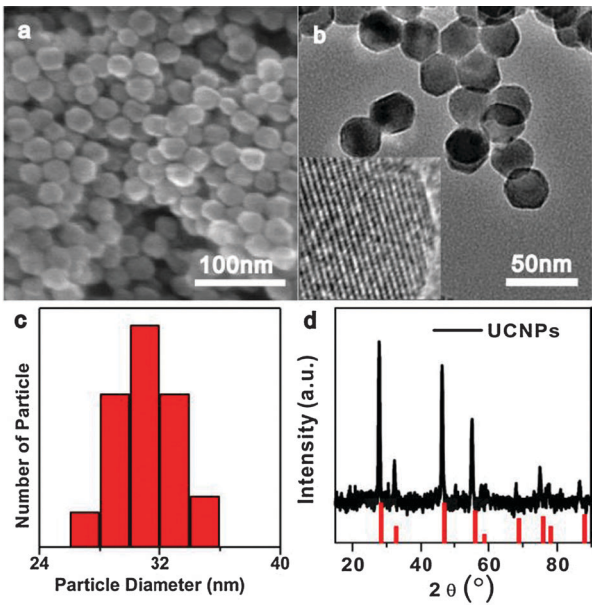

Fig. 1 (a) SEM and (b) TEM images of the $NaYF_4$:Yb^{3+}, Tm^{3+}–$NaYF_4$:Yb^{3+}, Er^{3+} core–shell nanocrystals (UCNPs). Inset: high-resolution TEM image of (b). (c) Histogram of the particle sizes obtained from TEM images of ~200 nanocrystals. (d) XRD patterns of the core–shell nanocrystals (UCNPs) and the standard patterns of pure cubic-phase $NaYF_4$ (JCPDS No. 06-0342, red line).

were formed under a certain temperature, the shell precursors were also transferred dropwise into the hot reaction flask in the same way as the addition of core precursors to generate cubic-phase $NaYF_4$:Yb^{3+}, Tm^{3+}–$NaYF_4$:Yb^{3+}, Er^{3+} core–shell nanocrystals. A more detailed description of the synthetic procedure is given in the Experimental section.

Fig. 1a and b are the typical SEM and TEM images of the resulting UCNPs. It can be seen from the TEM image that the synthesized particles are approximately 31 nm in diameter (Fig. 1c) and appear to be hexagonal in shape. The size is larger than that of the $NaYF_4$:Yb^{3+}, Tm^{3+} core nanocrystals which had a mean particle diameter of 23 nm (Fig. S1, ESI†). From the difference in particle sizes between the core-only nanoparticles and core–shell nanoparticles, it is thought that the observed increase in size of the core–shell nanocrystals is attributed to the growth of the $NaYF_4$:Yb^{3+}, Er^{3+} shell around the core. The crystalline structure of the products was further characterized using high-resolution TEM (HRTEM) and X-ray diffraction (XRD) analysis. HRTEM analysis of a single particle demonstrated that the distance between the adjacent fringes was 0.31 nm, which corresponds to the *d*-spacing for the (111) lattice plane in the cubic $NaYF_4$ structure.[45–47] The sharp peaks in the XRD pattern (Fig. 1d) indicate the good crystallization of the prepared nanocrystals. All the diffraction peaks could be well indexed to the JCPDS card No. 6-0342 of the standard cubic structure $NaYF_4$, and no peaks from other phases or impurities were observed. In addition, EDX analysis showed the presence of Y, Yb, Tm and Er in the $NaYF_4$:Yb^{3+}, Tm^{3+}–$NaYF_4$:Yb^{3+}, Er^{3+} core–shell nanocrystals, whilst there was no signal for Er in the sample of $NaYF_4$:Yb^{3+}, Tm^{3+} core nanocrystals (Fig. S2, ESI†). These results indicated that high-purity $NaYF_4$:Yb^{3+}, Tm^{3+}–$NaYF_4$:Yb^{3+}, Er^{3+} core–shell nanocrystals were obtained, which is very beneficial for obtaining bright luminescence.

3.2 Upconversion luminescence properties of the core–shell nanocrystals

The upconversion luminescence spectrum under the excitation of a continuous wave (CW) laser at 980 nm for $NaYF_4$:Yb^{3+}, Tm^{3+}–$NaYF_4$:Yb^{3+}, Er^{3+} core–shell nanocrystals presented in Fig. 2a shows multiple emission bands ranging from visible to NIR. The emission peaks at 520, 539, and 654 nm are assigned to Er^{3+} transitions from energy levels $^2H_{11/2}$, $^4S_{3/2}$ and $^4F_{9/2}$ to the $^4I_{15/2}$ ground state, respectively. The intense NIR emission at 802 nm is attributed to Tm^{3+} transition from $^3H_4$ to $^3H_6$. The dependence of the logarithm of the pumping power on the logarithm of the upconversion emission intensity is further investigated and shown in Fig. 2b. Both the slopes for the red and green emissions of Er^{3+} and the $^3H_4 \rightarrow {}^3H_6$ emission of Tm^{3+} are about 2, indicating a two-photo process, which are in agreement with data reported earlier.[46]

The prominent multiple emission bands of core–shell nanocrystals make them potential candidates for multifunctional bio-applications. It should also be noted that the luminescence of the core–shell nanoparticles was more intense than that of their co-doping counterparts (Fig. S3, ESI†). The visible emission can be utilized to indirectly excite photosensitizers for photodynamic therapy (PDT), while the NIR-to-NIR emission, which is located at the biological window, can be used for both imaging diagnosis and as a reference of fluorescence change. In the following work, we explored the application of the nanocrystals in PDT in detail.

3.3 PEG–phospholipid functionalization and photosensitizers loading on the $NaYF_4$:Yb^{3+}, Tm^{3+}–$NaYF_4$:Yb^{3+}, Er^{3+} core–shell nanocrystals (UCNP@PP–Ce6)

Due to the as-prepared $NaYF_4$:Yb^{3+}, Tm^{3+}/$NaYF_4$:Yb^{3+}, Er^{3+} core–shell nanocrystals bearing hydrophobic surface ligands of oleic acid (OA), it is unsatisfactory for their application in biomedical field. Amphiphilic poly(ethylene glycol)-conjugated phospholipid (DSPE-PEG 2000) was chosen to transfer these

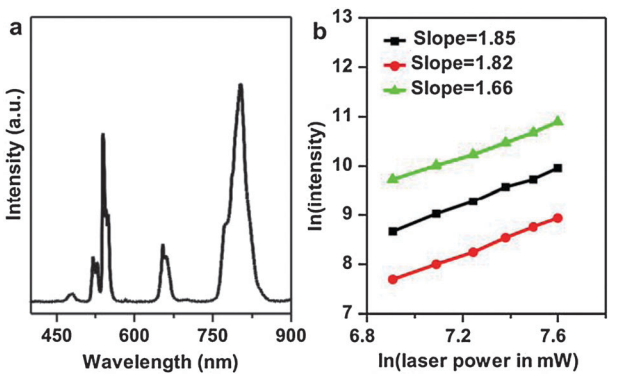

Fig. 2 (a) Emission spectra of UCNPs in cyclohexane upon excitation using a 980 nm laser diode. (b) Power dependence of the upconversion emissions of UCNPs on cyclohexane excited at 980 nm: a circle, a square and a triangle represent the transitions of $^4F_{9/2}$–$^4I_{15/2}$, $^4S_{3/2}$–$^4I_{15/2}$ and $^3H_4$–$^3H_6$, respectively.

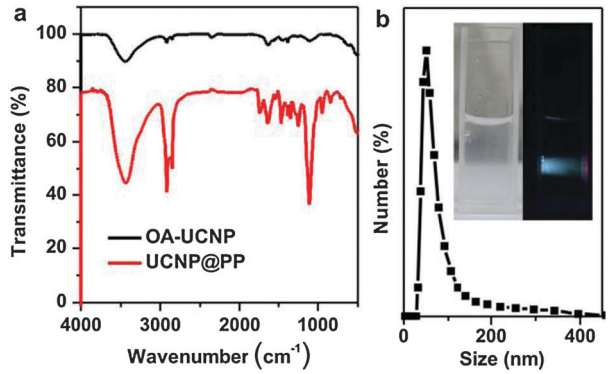

Fig. 3 (a) FTIR spectra of OA-UCNP (black curve) and UCNP@PP (red curve). (b) The size distribution of UCNP@PP nanoparticles in water. Inset: photographs of UCNP@PP nanoparticles in PBS under the ambient light and under a 980 nm laser excitation.

hydrophobic UCNPs into the aqueous phase. The successful DSPE-PEG 2000 coating on the surface of the UCNPs was verified using FTIR spectra. As shown in Fig. 3a, both of the oleic acid-coated UCNPs and DSPE-PEG 2000-coated sample (UCNP@PP) demonstrated a broad absorption band at around 3438 cm^{-1}, which corresponds to the O–H stretching vibration. Due to a large number of CH_2 groups in the DSPE-PEG coating, the IR peaks at around 2900 cm^{-1} were significantly increased in the UCNP@PP sample. In addition, some additional peaks from 1000 to 1400 cm^{-1} in the UCNP@PP sample were likely owing to the stretching vibrations of the C–O bond in PEG (Fig. S4, ESI†).

After surface modification, on one hand, the biocompatible, hydrophilic PEG groups of DSPE-PEG 2000 extend outward, rendering the UCNPs dispersible in water (inset of Fig. 3b). The size distribution of UCNP@PP in aqueous solution measured using dynamic light scattering (DLS) was about 51 nm (Fig. 3b). The increase in size compared with that of UCNPs (~31 nm) is due to the PEG–phospholipid shell. Also, after the surface modification of DSPE-PEG 2000, the UCNP@PP still retained a strong upconversion luminescence in aqueous solution (inset of Fig. 3b). On the other hand, the hydrophobic layer (composed of oleic acid and phospholipid) on top of the UCNP surface and beneath the PEG–phospholipid coating also endows the UCNP@PP as a functional carrier to load hydrophobic chemotherapeutic drugs or photosensitizers (PSs) for cancer cells. For the application of UCNPs in PDT, the maximum absorption peak of loading PSs should match the UCNPs emission well which affords the effective resonance energy transfer from UCNPs to PSs. Chlorin e6 (Ce6), a promising photosensitizer molecule for experimental photodynamic therapy with *Q*-band maximum absorption (650–700 nm) matching the 654 nm red emission of UCNP@PP, is loaded into the hydrophobic layer of UCNP@PP by physical absorption through simple mixing. The hydrophobicity of Ce6 facilitates its encapsulation into the inner layer of UCNP@PP.

As shown in Fig. 4a, the prepared UCNP@PP–Ce6 complex formed a yellow-green clear solution. The successful encapsulation of Ce6 into the UCNP@PP nanoparticles was also evidenced by the UV/Vis absorption spectra of UCNP@PP–Ce6, in which the characteristic Ce6 absorptions at about 400 nm and 650–700 nm

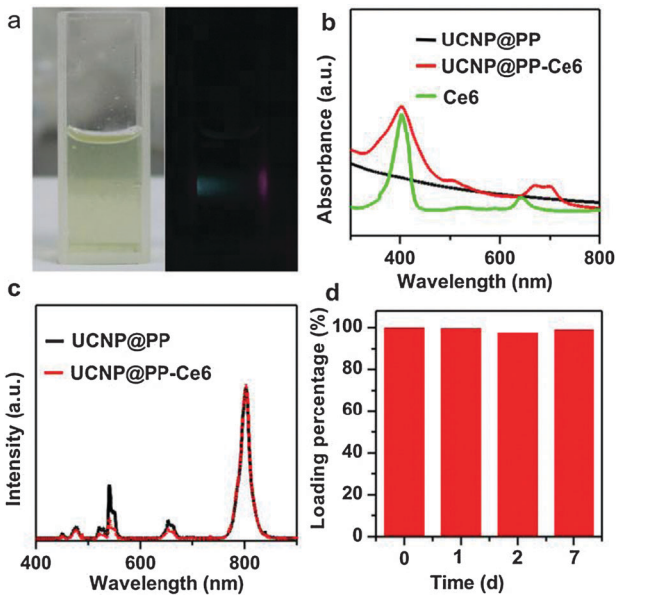

Fig. 4 (a) Photographs of UCNP@PP–Ce6 under ambient light (left) and under 980 nm diode laser irradiation (right). (b) UV-Vis absorption spectra of Ce6, UCNP@PP and UCNP@PP–Ce6 in PBS buffer (pH 7.40). (c) Upconversion luminescence spectra of UCNP@PP (black curve) and UCNP@PP–Ce6 (red curve). (d) The release of Ce6 from the UCNP@PP–Ce6 nanoparticles in PBS.

were clearly identified (Fig. 4b). According to the calibration curve of the UV-Vis absorption spectra of free Ce6 at 404 nm, the loading efficiency of Ce6 onto UCNP@PP in phosphate buffers (PBS, pH 7.4) was approximately 23% (w/w). In addition, after loading Ce6 into the nanoparticles, both the green and red emissions of UCNP@PP are strongly quenched, while the NIR (803 nm) band was not, owing to the resonance energy transfer from the UCNPs to the encapsulated Ce6 (Fig. 4c). The release of Ce6 from the UCNP@PP–Ce6 nanoparticles was also investigated in PBS solution (pH 7.40), sample solutions were taken on different days and centrifuged. The supernatants were subjected to UV-Vis absorption measurements. The results showed that Ce6 was not leaked from the UCNP@PP–Ce6 nanoparticles incubated in the PBS solution for up to seven days (Fig. 4d), suggesting that the nanoparticles are very stable against PS leaching. The excellent NIR emission and good stability against PS leakage of these nanoparticles make them a good candidate for various biological applications.

3.4 Determination of singlet oxygen

Singlet oxygen ($^1O_2$) is a highly reactive oxygen species and is believed to play a key role in the PDT. In this study, the singlet oxygen ($^1O_2$) production of UCNP@PP–Ce6 under the irradiation of a 980 nm laser was evaluated by an indirect chemical method using 1,3-diphenylisobenzofuran (DPBF). DPBF has an absorption peak at 420 nm and the intensity will decrease after interacting with singlet oxygen. As shown in Fig. 5, in the presence of UCNP@PP–Ce6, the absorption intensity of DPBF at 420 nm showed a significant decrease with the irradiation time (line 2), suggesting a high efficiency in generation of reactive $^1O_2$. In contrast, the change in the absorption intensity

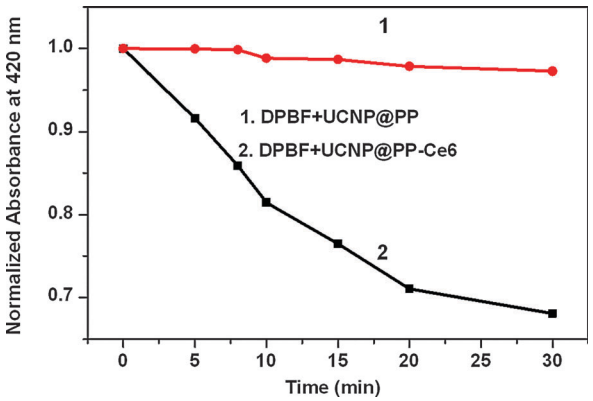

Fig. 5 Decay curves of the absorption of DPBF as a function of irradiation time. (1) DPBF with UCNP@PP and (2) DPBF with UCNP@PP–Ce6 in CH_3CN.

of DPBF was negligible in the absence of Ce6 (line 1). These results indicated that Ce6 was effectively activated by the emission from UCNPs and in turn caused the generation of singlet oxygen. Therefore, we investigated these Ce6-encapsulated UCNP@PP particles as a new PDT drug carrier in NIR-induced tumor therapy.

3.5 Cytotoxicity study and cell uptake

The cytotoxicity of these nanoparticles was first checked. The relative cell viabilities of human hepatoma cells (QGY-7703) and human hepatocytes (QSG-7701) incubated at different concentrations of UCNPs@PP–Ce6 for 12 h were measured using MTT assay. As shown in Fig. 6a, more than 70% of the cells survived after the co-incubation with 500 μg ml^{-1} UCNP@PP–Ce6 for 12 h, indicating that these nanoparticles are highly biocompatible. To monitor the intracellular uptake of Ce6 loaded UCNP@PP, HeLa cells were incubated with the UCNP@PP–Ce6 nanoparticles for 4 h. And then cells were imaged in the bright field and the fluorescence field using a confocal microscope. The green fluorescence from the Ce6 was observed at the cytoplasmic region of the cells (Fig. 6b). These results show the successful uptake of Ce6-loaded UCNP@PP nanoparticles by HeLa cell.

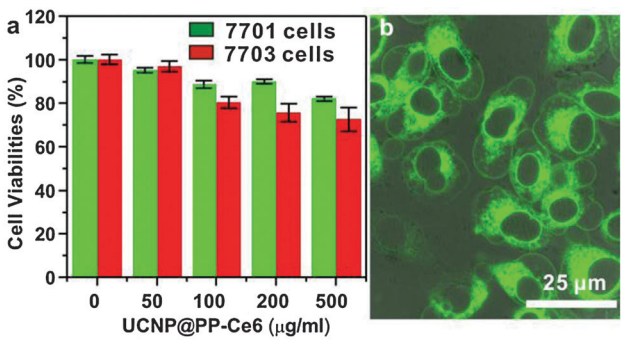

Fig. 6 (a) The viability of QSG-7701 liver cells and QGY-7703 liver cancer cells incubated with UCNP@PP–Ce6 at different concentrations, (±5)% of standard deviation. (b) Confocal fluorescence images of HeLa cells after incubation with UCNP@PP–Ce6 for 4 h.

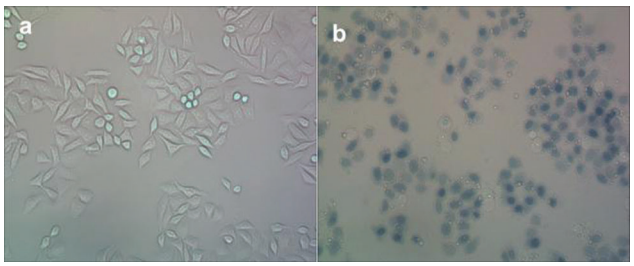

Fig. 7 Optical imaging of 7703 liver cancer cells stained with trypan blue: (a) with 100 μg ml^{-1} UCNP@PP–Ce6 and without 980 nm laser exposure; (b) with 100 μg ml^{-1} UCNP@PP–Ce6 and 5 min 980 nm laser exposure (1.5 W cm^{-2}).

3.6 *In vitro* PDT effects on cancer cells

Finally, the photodynamic effect of UCNP@PP–Ce6 on QGY-7703 cells was investigated. After incubation with 100 μg ml^{-1} of UCNP@PP–Ce6 for 12 h, the nanoparticle-treated cells were exposed to NIR light (980 nm laser) at a relatively low density of 1.5 W cm^{-2} for 5 min. The cells were then stained with trypan blue, a vital dye that only stains the cell when its membrane is damaged. There has been no cell death observed in all the control experiments (Fig. S5, ESI† and Fig. 7a), however significant cell death is observed for 7703 cells incubated with UCNP@PP–Ce6 after exposure to the NIR light for 5 min (Fig. 7b). Furthermore the cells with UCNP@PP did not show obvious damage with or without NIR light irradiation (Fig. S4c and d, ESI†). These results confirmed the PDT effects induced by the presence of Ce6 under NIR light irradiation. The absorbance of Ce6 at approximately 660 nm overlaps with the red emission peak of the upconversion NaYF4:Yb, Tm–NaYF4:Yb, Er nanocrystals, thus the light emitted by the nanocrystals activates Ce6 to release singlet oxygen species to kill the cancer cell.

4. Conclusions

In summary, core–shell structured $NaYF_4$:Yb^{3+}, Tm^{3+}–$NaYF_4$:Yb^{3+}, Er^{3+} upconversion nanocrystals (UCNPs) were synthesized with Tm^{3+} and Er^{3+} doped in the core and the shell, respectively, using a modified thermal decomposition method. Both NIR emission from Tm^{3+} and visible emissions from Er^{3+} were observed from the core–shell nanocrystals under the irradiation of a 980 nm NIR laser. After surface modification with PEG–phospholipid (PP), this water-soluble UCNP@PP could be used as a potential bio-label for *in vitro* and *in vivo* NIR optical imaging, and as a promising photosensitizer carrier for intracellular PDT. The prominent PDT effects of the UCNP@PP–Ce6 on the 7703 liver cancer cells demonstrate the promising prospect of UCNP@PP as a multifunctional nanoplatform for simultaneous diagnosis and therapy.

Acknowledgements

This work was supported by the National Natural Science Foundation of China (21101131, 21021061, 20925103), Natural Science Foundation of Fujian Province (No. 2012J01056), Fundamental Research Funds for the Central Universities (2010121015),

Scientific Research Foundation for the Returned Overseas Chinese Scholars of State Education Ministry and the NFFTBS (J1210014). We thank Dr Jianli Zou at Kyoto University for help with proofreading and Dr Binghui Wu for helpful discussions.

References

1 W. Jiang, B. Y. S. Kim, J. T. Rutka and W. C. W. Chan, *Nat. Nanotechnol.*, 2008, **3**, 145.
2 X. Michalet, F. F. Pinaud, L. A. Bentolila, J. M. Tsay, S. Doose, J. J. Li, G. Sundaresan, A. M. Wu, S. S. Gambhir and S. Weiss, *Science*, 2005, **307**, 538.
3 A. Burns, H. Ow and U. Wiesner, *Chem. Soc. Rev.*, 2006, **35**, 1028.
4 M. Liong, J. Lu, M. Kovochich, T. Xia, S. G. Ruehm, A. E. Nel, F. Tamanoi and J. I. Zink, *ACS Nano*, 2008, **2**, 889.
5 J. Kim, H. S. Kim, N. Lee, T. Kim, H. Kim, T. Yu, I. C. Song, W. K. Moon and T. Hyeon, *Angew. Chem., Int. Ed.*, 2008, **47**, 8438.
6 H. Zou, S. S. Wu and J. Shen, *Chem. Rev.*, 2008, **108**, 3893.
7 Y. Piao, A. Burns, J. Kim, U. Wiesner and T. Hyeon, *Adv. Funct. Mater.*, 2008, **18**, 3745.
8 F. Wang, X. L. Chen, Z. X. Zhao, S. H. Tang, X. Q. Huang, C. H. Lin, C. B. Cai and N. F. Zheng, *J. Mater. Chem.*, 2011, **21**, 11244.
9 X. J. Kang, Z. Y. Cheng, D. M. Yang, P. A. Ma, M. M. Shang, C. Peng, Y. L. Dai and J. Lin, *Adv. Funct. Mater.*, 2012, **22**, 1470.
10 F. Zhang, G. B. Braun, A. Pallaoro, Y. C. Zhang, Y. F. Shi, D. X. Cui, M. Moskovits, D. Y. Zhao and G. D. Stucky, *Nano Lett.*, 2012, **12**, 61.
11 H. Y. Xing, W. B. Bu, S. J. Zhang, X. P. Zheng, M. Li, F. Chen, Q. J. He, L. P. Zhou, W. J. Peng, Y. Q. Hua and J. L. Shi, *Biomaterials*, 2012, **33**, 1079.
12 Q. Liu, M. Chen, Y. Sun, G. Y. Chen, T. S. Yang, Y. Gao, X. Z. Zhang and F. Y. Li, *Biomaterials*, 2011, **32**, 8243.
13 L. Cheng, K. Yang, Y. G. Li, X. Zeng, M. W. Shao, S. T. Lee and Z. Liu, *Biomaterials*, 2012, **33**, 2215.
14 F. Wang and X. G. Liu, *Chem. Soc. Rev.*, 2009, **38**, 976.
15 Z. Q. Li, Y. Zhang and S. Jiang, *Adv. Mater.*, 2008, **20**, 4765.
16 Z. G. Chen, H. L. Chen, H. Hu, M. X. Yu, F. Y. Li, Q. Zhang, Z. G. Zhou, T. Yi and C. H. Huang, *J. Am. Chem. Soc.*, 2008, **130**, 3023.
17 G. Y. Chen, T. Y. Ohulchanskyy, R. Kumar, H. Agren and P. N. Prasad, *ACS Nano*, 2010, **4**, 3163.
18 G. S. Yi and G. M. Chow, *Chem. Mater.*, 2007, **19**, 341.
19 S. Heer, O. Lehmann, M. Haase and H. U. Güdel, *Angew. Chem., Int. Ed.*, 2003, **42**, 3179.
20 M. Wang, C. C. Mi, Y. X. Zhang, J. L. Liu, F. Li, C. B. Mao and S. K. Xu, *J. Phys. Chem. C*, 2009, **113**, 19021.
21 X. Teng, Y. H. Zhu, W. Wei, S. C. Wang, J. F. Huang, R. W. B. Hu, A. I. Y. Tok, Y. Han, Q. C. Zhang, Q. L. Fan, W. Huang, J. A. Capobianco and L. Huang, *J. Am. Chem. Soc.*, 2012, **134**, 8340.
22 X. M. Li, D. K. Shen, J. P. Yang, C. Yao, R. C. Che, F. Zhang and D. Y. Zhao, *Chem. Mater.*, 2013, **25**, 106.
23 X. Wang and Y. D. Li, *Chem. Commun.*, 2007, 2901.
24 D. K. Chatterjee, A. J. Rufaihah and Y. Zhang, *Biomaterials*, 2008, **29**, 937.
25 M. X. Yu, F. Y. Li, Z. G. Chen, H. Hu, C. Zhan and C. H. Huang, *Anal. Chem.*, 2009, **81**, 930.
26 Y. H. Wang, Z. J. Wu and Z. H. Liu, *Anal. Chem.*, 2013, **85**, 258.
27 M. Nyk, R. Kumar, T. Y. Ohulchanskyy, E. J. Bergey and P. N. Prasad, *Nano Lett.*, 2008, **8**, 3834.
28 N. N. Dong, M. Pedroni, F. Piccinelli, G. Conti, A. Sbarbati, J. E. Ramírez-Hernández, L. M. Maestro, M. C. Iglesias-de la Cruz, F. Sanz-Rodriguez, A. Juarranz, F. Chen, F. Vetrone, J. A. Capobianco, J. G. Sole, M. Bettinelli, D. Jaqué and A. Speghini, *ACS Nano*, 2011, **5**, 8665.
29 G. Tian, Z. J. Gu, L. J. Zhou, W. Y. Yin, X. X. Liu, L. Yan, S. Jin, W. L. Ren, G. M. Xing, S. J. Li and Y. L. Zhao, *Adv. Mater.*, 2012, **24**, 1226.
30 S. S. Cui, H. Y. Chen, H. Y. Zhu, J. M. Tian, X. M. Chi, Z. Y. Qian, S. Achilefu and Y. Q. Gu, *J. Mater. Chem.*, 2012, **22**, 4861.
31 W. Wei, T. C. He, X. Teng, S. X. Wu, L. Ma, H. Zhang, J. Ma, Y. H. Yang, H. Y. Chen, Y. Han, H. D. Sun and L. Huang, *Small*, 2012, **8**, 2271.
32 J. Zhou, Y. Sun, X. X. Du, L. Q. Xiong, H. Hu and F. Y. Li, *Biomaterials*, 2010, **31**, 3287.
33 D. K. Chatterjee and Y. Zhang, *Nanomedicine*, 2008, **3**, 73.
34 P. Zhang, W. Steelant, M. Kumar and M. Scholfield, *J. Am. Chem. Soc.*, 2007, **129**, 4526.
35 H. S. Qian, H. C. Guo, P. C. L. Ho, R. Mahendran and Y. Zhang, *Small*, 2009, **5**, 2285.
36 B. Ungun, R. K. Prud'homme, S. J. Budijono, J. N. Shan, S. F. Lim, Y. G. Ju and R. Austin, *Opt. Express*, 2009, **17**, 80.
37 H. C. Guo, H. S. Qian, N. M. Idris and Y. Zhang, *Nanomed.: Nanotechnol., Biol. Med.*, 2010, **6**, 486.
38 J. N. Shan, S. J. Budijono, G. H. Hu, N. Yao, Y. B. Kang, Y. G. Ju and R. K. Prud'homme, *Adv. Funct. Mater.*, 2011, **21**, 2488.
39 C. Wang, H. Tao, L. Cheng and Z. Liu, *Biomaterials*, 2011, **32**, 6145.
40 K. Liu, X. M. Liu, Q. H. Zeng, Y. L. Zhang, L. P. Tu, T. Liu, X. G. Kong, Y. H. Wang, F. Cao, S. A. G. Lambrechts, M. C. G. Aalders and H. Zhang, *ACS Nano*, 2012, **6**, 4054.
41 Z. X. Zhao, Y. N. Han, C. H. Lin, D. Hu, F. Wang, X. L. Chen, Z. Chen and N. F. Zheng, *Chem.–Asian J.*, 2012, **7**, 830.
42 F. Chen, S. J. Zhang, W. B. Bu, Y. Chen, Q. F. Xiao, J. N. Liu, H. Y. Xing, L. P. Zhou, W. J. Peng and J. L. Shi, *Chem.–Eur. J.*, 2012, **18**, 7082.
43 S. S. Cui, D. Y. Yin, Y. Q. Chen, Y. F. Di, H. Y. Chen, Y. X. Ma, S. Achilefu and Y. Q. Gu, *ACS Nano*, 2013, **7**, 676.
44 W. Spiller, H. Kliesch, D. Wohrele, S. Hackbarth, B. Roder and G. J. Schnurpfeil, *J. Porphyrins Phthalocyanines*, 1998, **2**, 145.
45 H. X. Mai, Y. W. Zhang, R. Si, Z. G. Yan, L. D. Sun, L. P. You and C. H. Yan, *J. Am. Chem. Soc.*, 2006, **128**, 6426.
46 J. C. Boyer, L. A. Cuccia and J. A. Capobianco, *Nano Lett.*, 2007, **7**, 847.
47 S. Heer, K. Kömpe, H. U. Güdel and M. Haase, *Adv. Mater.*, 2004, **16**, 23.

